Partial coherence and amplified internal energy when thermal radiation is sourced within matter

Journal of Physics Communications

OPEN ACCESS

RECEIVED
4 May 2022

REVISED
7 June 2022

ACCEPTED FOR PUBLICATION
14 June 2022

PUBLISHED
27 June 2022

PAPER

Partial coherence and amplified internal energy when thermal radiation is sourced within matter

G B Smith , A R Gentle and M D Arnold

School of Mathematical and Physical Sciences, University of Technology Sydney; Broadway, NSW, Australia

E-mail: geoff.smith@uts.edu.au

Keywords: anharmonic local resonance, ground state modes, photon thermal recycling, non-reciprocal emissivity, equilibrium balance, momentum conservation

Supplementary material for this article is available online

Abstract

Photons excited into ground state modes at finite temperature display partitioning among photon phases, lifetimes and distances travelled since creation. These distributions set the distance from an interface a created photon has some chance of emission. Excited photons have phase velocity set by their mode's propagation index n which sets mode density then internal energy contribution. All photons that strike an interface obliquely if emitted are refracted, and their exit intensities are irreversible except when weak internal attenuation occurs. Attenuation index k near zero degrees is small, so reversibility is approximate. As temperature rises refraction of exiting photons varies. Total emission remains reversible after transitioning through a nonequilibrium state with no other heat inputs. In equilibrium the densities of excitations that create and annihilate photons are in balance with photon densities, and emissivity dependent on n, k, temperature, and internal incident direction. Exit intensities from pure water and crystalline silica are modelled. They contain strong resonant intensities, and match data accurately. Intrinsic resonances formed within liquids and compounds are due to photon modes hybridising with localized excitations, including molecular oscillations and the anharmonic component of lattice distortions. They explain the many resonant spectral intensities seen in remote sensing. Each hybrid oscillator is a photonic virtual bound state whose energy fluctuates between levels separated by hf. Other features addressed are radiance when solid angle changes at exit, anomalous refraction, thermal recycling of internally reflected photons, fluxes within multilayers, and enhanced internal heat flux from phonon drag by photon density gradients under an external temperature gradient.

1. Introduction

1.1. Alternate models; classical, semi-classical and quantum

The models currently in wide use to predict spectral intensity profiles emerging from all heated matter, and their use to establish the total radiative cooling rates from a body in thermal equilibrium originated in Planck's resolution of the spectral intensity dilemma posed by emission from a cavity. An earlier prediction based on a classical thermodynamic treatment of total radiant power exiting a cavity by Stefan was not duplicated by Planck' initial photon model until he added a factor 2.0 to each intensity. Extensions to emission from condensed matter [1, 2] relied on various assumptions. Exit intensities were assumed to follow the energy conservation rule defined by a Kirchhoff emissivity acting on cavity emission, not from intensities created within a sample's volume but from quantum sources arrayed along its exit interface. Lambert [3] proposed this idea to explain the $\cos\theta$ directional profile in intensity he observed exiting a hot metal ribbon at angle θ to the normal. Planck assumed Lambert's profile was universal. In the volume models we present $\cos\theta$ is usually present, as interior based intensities are refracted at exit to conserve momentum of each transmitted photon. Cavity

emission is direct, so its intensities do not contain a cosθ factor. Had Planck used this he would not have needed to add to total exit intensity a factor of 2.0 to reproduce the correct classical power loss derived by Stefan.

For emission from materials Planck's cavity emission and the Kirchhoff rule emissivity retained the factor 2.0. We will show that hemispherical emittance ε_H based on cavity intensities modified by the Kirchhoff rule is not correct as exit refraction means exit mode intensities subject to internal loss are irreversible. Weak exit intensities in the limit that sample T approaches absolute zero are approximately reversible as each internal mode intensity has attenuation index k(f)∼0. Photons carried by modes within band gaps in semiconductors also create reversible exit intensities. At finite T photons impacting an interface and exiting must transfer into the neighbouring ground-state mode that ensures momentum conservation. That entry mode becomes temperature dependent as T and k(f) rise so reversal of exit fluxes at finite T does not retrace the original internal intensity. A blackbody component in all thermal radiation was justified by the entropy requirements of the *classical* version of the 2nd Law of Thermodynamics. Quantum thermodynamics allows single photon fluxes to be irreversible while maintaining reversibility of total exit radiant power $P_H(T)$, provided the original heat input rate dQ/dt is first removed. In equilibrium $dQ/dt = P_H(T)$ and temperature T is common to input and output, so both entropy fluxes match and the 2nd Law is obeyed.

The use of spectral absorptance A(θ,f) to define Kirchhoff emissivity $\varepsilon_K(\theta,f)$ was based on reversal of exit intensity I(θ,f,T) [4] at frequency f. This ignored exit refraction and neglected the thermal consequence of A(θ,f)I(θ, f, T). The volume-based intensity models in this paper prove that oblique emissivity $\varepsilon(\theta,f)$ from all matter is non-reciprocal at finite temperature whenever photons within a mode have a finite lifetime. Exit refracted photons are then irreversible upon transmitting into a neighbouring ground-state mode whose direction ensures conservation of photon momentum. The Kirchhoff-Planck (KP) model for thermal radiation from solids and liquids often gave approximate but inexact predictions of exit intensity data at finite T for intensities exiting out to $\theta < 65°$, which dominate intensities exiting at higher θ. Our models show errors from the use of $\varepsilon_K(\theta,f)$ based on reciprocity at finite T become more obvious as exit angle θ rises above 60°, and as photon lifetimes continue to reduce as temperatures rises. Effects omitted that led KP model responses to get close to some data but without exact fits include (i) internal critical angles associated with exit refraction (ii) the decrease in $\varepsilon(\theta,f)$ as internal reflectance rises (iii) the unnecessary addition by Planck of the factor 2.0 (iv) the assumption that Stefan-Boltzmann σ is universal. Our internal models show radiance intensity $I(T) = \sigma T^4\ Wm^{-2}$ is unique to the interior of a cavity while inside matter $I(T) = \kappa(\gamma T^4)\ Wm^{-2}$ where $\gamma = \sigma/(\pi^4/15) = 8\pi k^4/c^3h^3$ is a universal factor and κ a material specific numerical factor based on the densities of photons in each occupied ground state mode. The identity whose evaluation leads to κ appears in section 4 and has been applied to specific materials. The final factor needed is hemispherical spectral emittance ε_H so that total power emitted becomes $P_H(T) = A\varepsilon_H\kappa(\gamma T^4) = A\varepsilon_H I_H(T)$ W with A the exit area and $I_H(T)$ the total hemispherical intensity incident internally on the interface.

The usual approach to defining standing wave free modes inside matter is summarised in the Hamiltonian in equation (1). Each empty stationary mode is occupied by photons at finite T with spin σ photons, which are partitioned into modes at energy $E_{k*} = hf = h.c./\lambda$.

$$H_{ph}(k^*) = \sum_{\sigma} E_{k*,\sigma} c^+_{k*,\sigma} c_{k*,\sigma} = \sum_{\sigma} E_{k*,\sigma} n_{k*,\sigma} \tag{1}$$

$k^* = 2\pi n(\lambda)/\lambda = 2\pi n(f)f/c$ is the internal wavevector with n(f) this mode's wave index at frequency f. All photons in such modes in equilibrium have phase velocity c/n(f) and $n_{k*,\sigma}$ is the density of ground state modes with k^*_σ. Mode density $n_{k*,\sigma}$ has both directional and volume components. A thermally created photon can propagate in any direction from its creation point so directional densities are spherically symmetric, and the same for all modes at $E_{k*,\sigma}$ in the same material, and in different materials. Refraction means photons enter a neighbour's ground state mode that ensures momentum conservation. Volume density of modes at $E_{k*,\sigma}$ is defined by the impact of n(f) on $n_{k*,\sigma}$ in all bulk matter, using expressions available in section 4 based on free mode volume density $[4\pi k^3_*/3\ V]$ for each spin. If other interfaces are close enough to an exit interface of interest extra internal mode impacts occur which modifies mode density $n_{k*,\sigma}$. Each free particle density for matter occupying large enough volume V varies between modes at each $E_{k*,\sigma}$ and each mode density is material specific.

Energy partitioning is not the only photon distribution at finite T that must be considered. Each created photon is subject to subsequent time and location-based partitioning within its mode. Equivalently all photons present at any time within a mode have experienced a range of possible experiences governed by the phase velocity in that mode, its location along each mode when created, and the probability of survival to its current location. This probability of survival is statistical as it is governed by the distribution of photon lifetimes that occur within each mode. Each photon present has thus taken one of many available trajectories through time and space defined by its mode. The density of non-relativistic internal trajectories within all modes at $E_{k,\sigma}$ obeys a distribution function which is derived in section 3. Dual partitioning into energy then into past or future transport outcomes over time is a central feature of quantum thermodynamics. Time dependence in quantum

ground state modes involves internally or externally driven quantum energy exchange between two distinct ground states. In our case the pair of ground states can be an extended mode that is transporting many phonons and one that transports many photons, or that carrying photons exchanging energy with a local valence defect or local oscillator. Dynamic exchange between two local quantum modes and an external oscillator as a function of temperature is of recent current interest for control of entanglement between qubit atoms, using a two mode Rabi model [5–7]. Photon dissipation rates due to energy exchange between photon modes and either phonon modes or arrays of local oscillator modes in thermal equilibrium underpins this paper's models of the quantum information present in all thermal radiation due to variable rates of such dissipation. At finite T photons are distributed among time dependent sub-modes defined by three quantum properties k^*, σ, m per mode with m a photon transport variable in equilibrium. It can be phase ϕ(f), lifetime τ(f) or distance travelled d^*(f) since creation for each photon.

$$H_{k^*,\sigma,m} = \sum_{\sigma} E_{k*,\sigma} \sum_{m}^{n_{k*,\sigma}} c^{+}_{k*,\sigma;m} c_{k*,\sigma;m} = \sum_{\sigma} E_{k*,\sigma} \sum_{m}^{n_{k*,\sigma}} m_{k*,\sigma;m} \tag{2}$$

Equation (2) then represents solutions of a time-dependent Schrödinger equation with a time dependent dissipation term. Phase ϕ(f,t) for each photon at time t is also defined by a photon's location along its mode defined by $\phi(d^*(f),t)$. Photons at energy $E_{k*,\sigma}$ can be partitioned according to their values of τ(f), d^*(f) and phase change experienced by each photon since its creation. Various balances in equilibrium are required to define the equilibrium distribution of photons present in one mode among these and related properties. The required balances are listed in section 2 and include the balance between rates of creation and of annihilation from energy exchange, for example between a phonon mode and oscillations on a local molecule. That balance ensures the volume density N(f,T) of photons in energy modes in any direction at $E_{k*,\sigma}$ and occupancy of each [k_*,σ;m] sub-state at $E_{k*,\sigma}$ is stable. Equilibrium also requires that at any instant the time-averaged distribution function of photons among [k,σ,m] sub-states, for example by their phase, is also stable. $m_{k*,\sigma;m} = c^{+}_{k*,\sigma,m} c_{k*,\sigma,m}$ is the density of photon ground states at mode energy hf and spin σ available to photons with specific transport property m as temperature T is varied. The function we derive here describing photon partitioning among the m states within $n_{k^*,\sigma}$ also provides a precise measure at each T of the partial coherence present in a photon mode. The rates that $c^{+}_{k^*,\sigma;m}$ and $c_{k^*,\sigma;m}$ operate are in dynamic balance in equilibrium. The equilibrium optical intensities and temperatures resulting define the transport outcomes within each mode that can be observed and used for model validation and in optical and thermal predictions. Partial coherence among the photons within a mode can also be observed.

Photon modes that strike an interface do not split. Their photons instead enter pre-existing modes, one in the initial material, the other in the material entered. The modes entered ensure that photon transfer conserves momentum. Those that tunnel to a mode in the next medium change their n(f), k(f) values so the mode they enter is defined by a complex Snell's law connecting internal incidence angle θ^* to exit direction θ. Ground state modes can be defined using Maxwell EM waves when fluxes are not attenuated as T approaches 0 K. When T rises k(f) also rises so the neighbouring ground-state mode entered is temperature dependent as refraction depends on n and k, and unless k(f)~0 exit mode intensities are irreversible (see sketch in the supplement available online at stacks.iop.org/JPCO/6/065004/mmedia). Optical phase changes following reflection by an interface do not modify phase distribution functions at finite T as each photon's phase shifts by the same amount.

A few models have addressed generation of thermal radiation inside matter. Their fundamentals differ to those in this paper, though there are common aspects. One used the semi-classical electromagnetic radiation from fluctuating electrical currents [8, 9] as defined by the fluctuation-dissipation (FDT) model's treatment of thermally excited quantum currents [10, 11]. Another addressed an example of the many different spectral resonant features seen in remote sensing of minerals [12]. The link of the Lorentz-Lorenz dispersion treatment of a classical oscillator to a material's complex refractive indices n(f), k(f) was used after general oscillator parameters had been fitted to observed emission spectra. The resulting n(f), k(f) for quartz matched known optical values. Their internal reflectance of obliquely incidence internal fluxes showed the Kirchhoff emissivity did not predict exit intensities though exit mode refraction was not addressed. Our models predict that special directional and spectral intensity characteristics occur after refraction of fluxes whose frequencies are near resonance. We include the role in equilibrium of photon thermal recycling following internal interface reflectance. Most alternate models do not address this issue, as they were surface based.

1.2. Intrinsic resonant emission in thermal radiation

Resonances within thermal radiation can be seen exiting most liquids, pure crystalline lattices, and matter containing local defects such as the vacancies and interstitials found in non-stoichiometric compounds such as TiN_x and $Ti_yAl_{1-y}N_x$ [13–15]. These resonances occur when ground state internal normal modes can hybridise with a local oscillator mode. Each mode photon can enter the hybrid for the resonance period, when extra photons are produced, and all finally return to the propagation mode. The supplement has further details on the

mixing Hamiltonian involved and how a photon that enters causes a local gain in the flux of energy at hf as exit flux of photons at hf is amplified at exit. In pure crystalline matter a high density of such hybrids per mode forms so their combined exit mode intensities display strong resonant features. Two examples of strong resonant features our models precisely predict follow for (i) water where resonance occurs exactly at the known molecular mode frequencies (ii) a stoichiometric silica lattice. In crystalline matter harmonic distortions of each bond propagate as phonons, but are accompanied with localized anharmonic distortions that can hybridise with a photon mode of energy hf. Each local resonance occurs between energy levels E_A and (E_A+hf) with E_A the energy of each anharmonic distortion which occur at high density in stoichiometric silica [12] and silicon carbide [16]. The relative time a photon spends at energies E_A and (E_A+hf) relates to its energy gain at resonance. Intrinsic resonances within thermal radiation give precise spectral and chemical bond details, and occur inside liquids, solid dielectrics, many compound conductors and crystalline lattices.

1.3. Photon transport statistics in each mode

Section 3 covers the statistical distribution of equilibrium photon transport properties within the m states introduced in equation (2). As above they include distances $d^*(f)$ travelled by each photon still present since its creation, and photon lifetimes $\tau(f)$. The distribution of these properties obeys well-defined rules based on equilibrium balances [17]. They have mean values such as $\langle d^*(f)\rangle$ the mean-free-path which is a feature of distribution function $P(d^*(f))$ for each material. Equilibrium balance between creation and annihilation rates ensures that these distribution functions are stable and unique to each mode. They can be related directly to optical properties such as $\alpha(f)$ the optical absorption coefficient for each material. $P[d^*(f)]$ provided us a proof that almost all emitted photons are created with a distance $d^*(f) \sim 7.5\langle d^*(f)\rangle \sim 7.5[1/\alpha(f)]$ from an exit interface on a bulk single material, as $d^*(f)$ spans values from near zero to a maximum $d^*(f)_{max}$. $P(d^*(f))$ ensures internal propagation usually occurs prior to emission and is derived and plotted in section 3. It allows us to set $d^*(f)_{max}$ for each different material for a desired accuracy.

Photons and other thermal excitations such as phonons co-exist at finite T. The non-photon excitations that create and annihilate photons determine photon density in each mode and $\langle d^*(f)\rangle$ [17]. An addition to standard internal heat flow when an external temperature gradient is applied occurs as internal balance requires that a photon gradient matches an accompanying phonon gradient when loss and gain occur in photon-phonon collisions. 'Phonon drag' by photons follows. Ground state mode directions within composite materials are initially uniform in each component material but mode topology changes if additional close interfaces allow created photons added to a mode to have more than one chance of transfer into a neighbouring medium. Confusion also arises at finite T because the two ground state modes each photon can enter at an interface are another mode in its starting material or one in a different direction in the neighbouring material. These two choices result from momentum conservation hence a complex Snell's Law. Confusion results as *the mode entered within the neighbour is a function of temperature.* That is the new direction and intensity depend on n(f), k(f) in the two neighbours at the same T. Only in the external continuum is k(f) fixed at $k(f) = 0$ as T rises.

The modelling principles we develop for bulk linear modes are readily extended to those in more complex internal structures, in particular multilayers, and select composites. Thermodynamic balance always requires the photon density along each mode whether linear or contoured to have well-defined $P(d^*(f))$, $\langle d^*(f)\rangle$ and photon fluxes at each frequency. The rates at which photons enter from a neighbouring mode or leave to adjacent matter affect these responses. The local volume density of photons is no longer uniform if modes allow multiple escape chances into neighbouring modes along with the possibility of multiple internal reflections. Flux intensities and internal energy density matched when straight modes applied in all directions, but they become decoupled once the probabilities of multiple reflections are finite. Unlike classical many particle problems different local volume densities are allowed at finite T in quantum particle systems as balance involves thermal diffusion within modes not between them. Internal energy densities U(T) must then be worked out for each different composite structure. An example application of these principles to a structure with two internal interfaces and a note on what can be learned about internal mode structure generally from observation of external intensities $I(\theta,f,T)$ is in the supplement.

$P(d^*(f))$ defines the quantum information carried by thermally excited photons and shows that partial coherence per mode can be controlled and engineered by setting dissipation rates as they are governed by quantum energy exchange between extended or localized non-photon modes and photon modes. Quantum processes that drive the transition from a noisy, chaotic beginning to thermal equilibrium reduce noise content over time until balance sets in between creation and annihilation. Residual noise in equilibrium exit modes can also occur and will be demonstrated. Maxwell wave model treatments of thermal radiation, with FDT modifications added, have some common features to our quantum models. The FDT approach to photons is semi-classical and arose from the description of the response of thermally excited electrons subject to random ohmic loss within matter under applied fields. The resulting currents displayed Johnson noise(8–10). For FDT

models of photon fluxes to reproduce the partial coherence and external thermodynamic equilibrium intensities predicted in this paper, they must incorporate exit refraction plus the thermodynamic balance rules following in the next section. A symbol glossary is included before our reference list as we are introducing concepts that may be unfamiliar to those used to standard thermal radiation models. The table also contains a useful summary of the physics used and introduced. The main study is broken up into seven parts; sections 2, 3 and 4 address core physical concepts needed to define internal intensities and energy; sections 5, 6, and 7 address the resulting optical and thermal responses. and the quantum information present in exit intensities. The data predicted is observable and useful for model validation.

2. Equilibrium intensities and precursor non-equilibrium states

Non-equilibrium photon fluxes are irregular and precede the formation of the more regular transport properties in equilibrium. Photons flowing in transient and stable regimes have the same phase-velocity per mode, but transient densities are not in balance with the non-photon excitations within modes photons can lose energy to, or gain energy from, their excitations. The distribution of lifetimes per photon in each mode at finite T and energy hf influences the equilibrium spectral intensities within each mode, and photon densities. Initial focus is on spectral intensities within bulk pure matter and the equilibrium intensities moving into the external mode that ensures each photon's momentum and energy are conserved. To exit photons tunnel through a terminating reaction potential into the required continuum mode. The Kirchhoff rule did not account for exit refraction despite mode indices n(f) and k(f) changing upon exit as all exit photons were created on the exit interface. Absorptance of reversed exit intensities to define emissivity also ignored outcomes from the additional heating rate δ(dQ/dt) it creates, with dQ/dt the heating rate that led to the equilibrium state at $T = T_0$ and output energy flux $P_H(T_0)$. Refraction at finite T always involves photons joining an adjacent mode in a different direction, which becomes increasingly irreversible as attenuation index k(f) grows and emissivity becomes more non-reciprocal. The mathematical definition of oblique emissivity when k(f) is finite is derived rigorously in section 5 and never matches $A(\theta,\lambda)$. Refraction also traps internal propagating photons striking the interface above any internal critical angle θ^*_C(f) due to total internal reflection (TIR), which adds to the internal thermal recycling of reflected photons whose $\theta^* < \theta^*_C$(f).

Standing wave modes in samples with only one interface and sufficient size to be opaque, are linear and directionally spherically symmetric, but modes within multilayers and composites will display non-linear modes. A transmitting slab is the simplest example as its internal modes follow zig-zag paths between opposite interfaces as used by McMahon [18] and Kollyuk *et al* [19]. Some features they predict are found in our models, but basic errors occurred in both of these studies (see supplement), despite approximate agreement with select experimental intensities. One did not include loss from both sides [19], both neglected refraction and detailed balance within their zig-zag modes [18]. Partial but inexact agreement with select optical data is common in older thermal radiation models despite their various errors which partially cancelled each other (see list above). Volume density of photons in equilibrium within extended linear modes is our starting point. Modifications for added interfaces depend on interface spacings. The supplement introduces this issue for multilayers as an additional statistical transport property arises, the probability a mode photon impacts an interface w(f,θ^*) times before it is finally annihilated or exits. θ^* is the initial angle of incidence per mode to the next interface struck which affects the spacing of each arm of the whole zig-zag mode and its volume density. Photon density *along* a contoured mode is constant in equilibrium, but volume density depends on w(f,θ^*) as well as n(f), T, θ^*, and the spacing between interfaces.

Partial coherence in a mode emerges soon after initial heating, gets stronger, and finally stabilises. When a mode's annihilation rates rise equilibrium phase coherence content grows, which is classically counter-intuitive but central to quantum thermodynamics. A related and possibly more puzzling corollary for classical physics is that as temperature increases photon internal annihilation rates rise as index k(f) rises. The degree of photon coherence within a mode then grows. The primacy of Maxwell's models in the study of thermal radiation rather than photonic thermodynamics, was suggested by Mischenko [20, 21]. That is not supported by our quantum thermodynamic models of modal fluxes whose empty stationary wave modes take account of all internal potentials that influence photon transport. Ground state solutions for nearly empty modes at $T \sim 0$ K when occupied at higher T should not be confused with the 'rays' used in geometric optics. Each half of a standing wave solution at finite T carries matching but opposite energy fluxes. A Maxwell wave's amplitude and intensity reduces with distance travelled internally, as defined by absorption coefficient α(f), and is related to the survival probability of a photon with distance travelled from its random creation location in its mode. In thermal equilibrium at finite T, the following dynamic balances within and between fluxes are required. Predictions of individual flux intensities and equilibrium thermal outcomes all require the first three internal balances to be present.

(i) photon densities N(f,T) and densities M(f,T) of the excitations or defects present which create photons and are created when photons [17] are annihilated. The rates photons are created and annihilated in equilibrium depend on M(f,T) so rates of creation and annihilation are in dynamic balance.

(ii) the rate internal photons are recycled by internal reflectance at each interface and the rate these internally reflected photons are annihilated and add heat

(iii) the macroscopic rate of heat input dQ/dt and total power radiated $P_H(T)$
Equilibrium balances (i), (ii), and (iii) apply within single materials and composites. An extra balance (iv) is needed for samples which have additional internal interfaces to the exit interface. They include transmitting slabs, coated substrates, multilayers, and matter containing particles or pores.

(iv) The rates that a mode's photons within each different material are lost by annihilation, by transmission to the next material, including to free space if applicable, and the rate all lost photons are replaced by creation events.

Resonances that result within samples with internal interfaces are structure based and distinct from the intrinsic anharmonic, bond defect and molecular resonances mentioned above. Outputs from some materials can inexactly approximate the spectral predictions of the Kirchhoff rule's predictions of resonant outputs from transmitting layers [18, 19] as their various errors partially cancel each other. The conclusion lists select historical examples where the Kirchhoff model could not be reconciled exactly with data, even when its predictions were approximate. Other balances to those just listed can occur, for example when photons are inducing motion in nearby particles or molecules.

Internal photothermal recycling in equilibrium can significantly impact all intensities. Due to the past focus on sources confined to an interface it was bypassed. Recycling followed by absorption resets equilibrium and internal energy density. Sample thermal mass C does not change but the thermal response to input dQ/dt does change, as internal heating rate is amplified. For a sample initially at ambient $T = T_A$, the expected stored heat change is $\Delta Q_0 = C(T_0\text{-}T_A) = C\Delta T_0$ but annihilation of internally reflected photons adds heat so in balance total stored energy becomes $\Delta Q^*(T) = C(T\text{-}T_A) = C\Delta T$ with $T > T_0$ and $\Delta Q^*(T) = \Delta Q_0/(1\text{-}R_H) = \Delta Q(T_0)/\varepsilon_H$ (a proof is in the supplement). Internal hemispherical reflectance R_H acts on internal hemispherical radiance $\Lambda_H(f,T)$ $Wm^{-2}Sr^{-1}$ made up by projections $\Lambda(\theta^*,f,T) = \Lambda(f,T)\cos\theta^*$ onto the interface as $\Lambda(f,T)$ is uniform. Thus $\Delta T/\Delta T_0 = 1/\varepsilon_H$ as internal heating rate is amplified. Heat generated by annihilation of recycled photons means equilibrium excitations M(f,T) and N(f,T) remain in balance but are amplified. Such changes must be accounted for in models of radiative cooling, and spectral and directional properties of external intensities. Total input and output entropy flows also change but remain in balance. In terms of externally applied heating rate dQ/dt a hybrid thermal heat capacity $C^*(T)$ determines equilibrium temperature T. Without recycling the usual result is $\Delta T_0 = (dQ/dt)/C$, but with recycling $\Delta T = (dQ/dt)/[(1\text{-}R_H)C] = \Delta T_0/\varepsilon_H$ so hybrid heat capacity $C^*(T) = [(1\text{-}R_H)C]$ sets T. Since $C^*(T) = \varepsilon_H C(T)$ accurate ε_H is important, whether from calorimetry, or directional emissivity. To the usual sensitivities governing C(T) we add for $C^*(T)$ the influence of R_H, any extra internal interfaces and exit surface topology. As ε_H approaches its 'white' limit of zero $C^*(T)$ also approaches zero and internal energy becomes quite large at fixed dQ/dt. Near the blackbody limit $\varepsilon_H \sim 1$, $C^*(f) \sim C(T)$ and neglect of internal recycling becomes a reasonable approximation.

The diverse sensitivity of exit intensities and directions to frequency are accurately predicted by our models. ε_H governs radiative cooling rate $P_H(T)$, but it is $\varepsilon_H\kappa\gamma T^4$ not $\varepsilon_{H,K}\sigma T^4$ from Kirchhoff-Planck models. $\gamma = (15/\pi^4)\sigma = 0.15399\sigma$ with σ the Stefan-Boltzmann constant. κ is a material specific constant arising from each $I_H(f,T)$ and $\Lambda_H(f,T)$ projected onto the interface as $\Lambda(f,T)\cos\theta^* d\Omega(\theta^*)$ and summed over a hemisphere, which gives $0.5\Lambda(f,T)$ (noting both spins are already accounted for in $\Lambda(f,T)$). For exit from a hole in a cavity wall $\Lambda(f,T) = \Lambda_{BB}(f,T)$ and projection factor $\cos\theta^*$ plays no role. The summation over frequency to model $I_H(f,T)$ and $\Lambda_H(f,T)$ is presented in the supplement. It uses our spectral density models in section 4 based on $x(f,T) = hf/kT$. $P_H(T)$ from accurate calorimetry does not change but $\varepsilon_H = 6.4939\varepsilon_{H,K}/\kappa$ can differ from $\varepsilon_{H,K}$. Errors depend on the material and the interface topology. Starting with stationary ground state internal modes also avoids the need to use near fields induced by Maxwell waves at interfaces. The evanescent modes that traverse sub-wavelength pores and gaps between solid layers, or a small gap between a substrate and a nearby small particle or molecule are defined by the external extent of the reaction potential per mode at each interface. Whether fluxes emerge within internal gaps from these potentials depends on the size of gaps relative to the span of the potential which has the sharp form $A(f)/r^6$ as the Hamiltonian has an added 'dipole-image dipole' reaction potential at the entry edge of any gap. The extent of this potential into a gap sets the probability an impacting photon is reflected, radiated across the gap, or transfers non-radiatively into the next material.

The distribution function $P(d^*(f))$ is based on $\langle d^*(f)\rangle$ from figure 1 next section. It also defines the spread of photon phase changes $\Delta\phi(f)$ since creation for each photon present in terms of mean phase change $<\Delta\phi(f)$. The

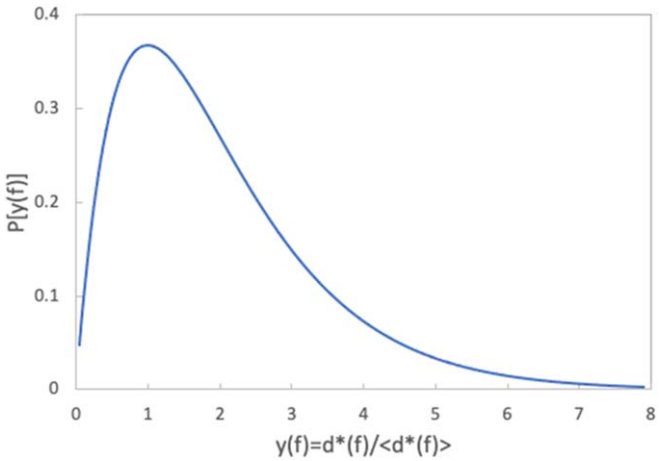

Figure 1. The distribution function within matter of distance travelled by each photon present from its creation point. Other photon internal transport properties subject to photon annihilation plus creation follow the same distribution function.

spread of all photon phases per mode at any instant also requires creation and annihilation rates to balance [17]. The function $P(\phi(f)/\langle\phi(f)\rangle)$ includes the phase of all photons making up photon density N(f,T). $P(\phi(f)/\langle\phi(f)\rangle)$ and $P(d^*(f)/\langle d^*(f)\rangle)$ supply a variety of quantum information including the value of $d^*(f)_{max}$, the partial coherence among photons within each mode and the proof that almost all emitted photons are created within a distance $d^*(f) \sim 7.5\langle d^*(f)\rangle \sim 7.5[1/\alpha(f)]$ from an exit interface. Both distributions are derived and plotted in the next section.

For a single material the magnitude of internal wavevector $k^* = 2\pi n(\lambda)/\lambda$ influences transmitted and reflected intensities at the exit interface. Its use to model a mode's contribution to volume density is described in section 4 which is focussed on large single material matter in equilibrium. It's modes are linear and directionally spherically symmetric. Two useful optical identities that both prove that $\varepsilon(\theta,f)$ for a single material is non-reciprocal follow in section 5. One replaces the Kirchhoff model for $\varepsilon(\theta,f)$ given by $A_{TM}(\theta,f)$ or $A_{TE}(\theta,f)$ the spectral absorptances of reversed exit fluxes for each polarisation. We prove that $\varepsilon(\theta,f) = |t_{TM}(\theta^*,f)|^2$ or $|t_{TE}(\theta^*,f)|^2$ for each internally incident intensity with $t(\theta^*,f)$ the usual Fresnel transmittance coefficient. $|t(\theta^*,f)|^2$ never matches the Kirchhoff spectral absorptance $A(\theta,f)$ of a reversed exit flux except when $\theta^* = 0°$. Reversal of oblique exit spectral intensities leads instead to internal intensities in directions different to θ^* to the normal unless $k(f) = 0$. Relevant schematics are in the supplement. The replacement emissivity acts on internally incident spectral intensities and the result accurately predicts the diverse spectral intensity characteristics exiting ionic and molecular materials. If IR indices n(f), k(f) are available no adjustable parameters are needed for accurate predictions.

3. Statistical transport properties that define partial coherence and require internal propagation to precede emission

The distribution function $P(d^*(f))$ models the probability that any photon present has travelled internal distance $d^*(f)$ from its random creation location within a transporting mode. A similar function describes classical scattering loss from a beam of molecules with distance travelled by the beam [22]. Quantum particle properties are different being a combination of photons not yet annihilated and those created to maintain equilibrium in place of those annihilated within a typical sampling time. That means at any one time in equilibrium a span of $d^*(f)$ per photon from 0 to $d^*(f)_{max}$ follows a fixed distribution function $P(d^*(f))$ of photon density as a function of $d^*(f)$. A formal derivation of mean-free-path $\langle d^*(f)\rangle$ follows in this section after the derivation of $P(d^*(f))$. Internal intensity retains noise spikes, but they are not usually detected in intensity data sampled over time periods of femtoseconds or longer for mid-IR radiation. A pictorial rendition of one set of creation events within $d^*(f)_{max}$ of an interface follows. It includes an example of exit noise when a photon is annihilated within $d^*(f)_{max}$ of an interface but not replaced by a compensating creation before its initial $d^*(f)_{max}$ cohort exits. The number of photons present per unit volume that have survived transport over distance $d^*(f)$ is $\Delta N(d^*(f)) = N(f,T)[\exp(-\alpha(f)d^*(f)]$ while $N(f,T)-\Delta N(d^*(f))$ are the photons lost which on average are compensated by creation of $N(f,T)[1-\exp[-\exp(\alpha(f)d^*(f))]$ photons at random locations along the same mode. The survival density function $\rho(d^*(f)/N(f,T) = [d(\Delta N(d^*(f))/d^*(f)] = -\alpha(f)\exp[-\alpha(f)d^*(f)]$. $\rho(d^*(f))$ is the density of mode photons that reach the range $d^*(f)$ to $[d^*(f)+\Delta d^*(f)]$ from where they started at initial time $t=t_0$ where the density was N(f,T). The initial set of

N(f,T) photons start out at a variety of initial locations along the mode at E = hf. $\rho(d^*(f) = n_{k^*,\sigma,d^*}$ of equation (2) after setting property $m = d^*(f)$ and its occupation is from $n_{k^*,\sigma,d^*} f_{BE}(f,T)$ the density of photons that have travelled $d^*(f)$ over the time interval $\Delta t = (t\text{-}t_0)$. Mean loss occurs at $d^*(f) = \langle d^*(f)\rangle$ using $\rho(d^*(f) = [d(\Delta N(d^*(f))/d^*(f)]$. Temporarily replacing $d^*(f)$ with d^* to compress the integrals in equation (3) gives

$$\langle d^*(f)\rangle = \int_0^\infty d^*\rho(d^*)d(d^*) - \int_0^\infty d^*[-\alpha(f)\exp(-\alpha(f)d^*)]d(d^*) \tag{3}$$

Carrying out the definite integration and requiring optical intensities to be based on energy fluxes per mode leads to these optical identities for mean-free-path per mode

$$\langle d^*(f)\rangle = \frac{1}{\alpha(f)} = \frac{\lambda/2\pi}{\varepsilon_2(f)} = \frac{c}{\sigma(f)} = \frac{\delta(f)}{n(f)} \tag{4}$$

$\rho(d^*(f))$ can be made generic to any mode in any material by transforming to scaled distance unit $y(f) = d^*(f)/\langle d^*(f)\rangle = \alpha(f)d^*(f)$. This is a universal survival distance along modes in which photons are annihilated when $\alpha(f)$ is finite. After transforming $d(d^*(f))$ to $\langle d^*(f)\rangle dy(f)$ the second integral in equation (1) becomes

$$-\langle d^*(f)\rangle \int_0^\infty dy(f)\{y(f)\exp[-y(f)]\} = \langle d^*(f)\rangle \int_\infty^0 dy(f)P(y(f)) \tag{5}$$

The integral over $P(y(f)) = P[d^*(f)/\langle d^*(f)\rangle]$ is normalized so $P(y(f))$ represents a probability density of photons present that have travelled (or will travel) $d^*(f)/\langle d^*(f)\rangle$ universal distance units over any time-period less than the maximum possible photon lifetime $\tau(f)_{max}$ in that mode. The alternate optical parameters in equation (4) that also define $\langle d^*(f)\rangle$ are $\varepsilon_2(f) = 2n(f)k(f)$, $\sigma(f)$ the optical conductivity, and $\delta(f)$ the skin depth. $r(d^*(f) = n_{k^*,\sigma,d^*}$ of equation (2) after setting sub-mode property $m = d^*(f)$. $P(y(f))$ is a universal probability density applying to all photons within a mode at any hf and is plotted in figure 1. It guides the setting of $d^*(f)_{max}$ as a chosen pre-set $y(f)$ upper limit based on desired accuracy and sets the $d^*(f)$ cut-off beyond which a photon's transport becomes negligibly small. That means $d^*(f)_{max}$ sets the maximum distance from an interface a photon can be created and have a chance of being emitted. $\langle d^*(f)\rangle$, $P(d^*(f))$, and $d^*(f)_{max}$ are material specific properties that depend on annihilation rates. $P(y(f))$ means photons emitted are mainly thermally created in the range $0.25\langle d^*(f)\rangle$ to $2.5\langle d^*(f)\rangle$ from an interface.

The function $P(y(f))$ also defines the partial coherence within each mode as it measures the phase correlation between individual photons in modes at hf. Each photon present reaching $d^*(f)$ from creation has undergone a phase change $\Delta\phi(f) = 2\pi f[d^*(f)/c^*(f)]$ with phase velocity $c^*(f) = c/n(f)$. Averaging phase changes per photon over all photons present the mean-phase-change is $\langle(\Delta\phi(f)\rangle = 2\pi f\{n(f)\langle d^*(f)\rangle/c\}$ or $(2\pi/\lambda)[n(\lambda)\langle d^*(\lambda)\rangle/\alpha(\lambda)]$ in terms of wavelength. The distribution function $P(\langle(\Delta\phi(f)/\langle\Delta\phi(f)\rangle)$ thus duplicates $P(y(f))$ of figure 1. Partial coherence within each absorbing mode follows once $\langle\Delta\phi(f)\rangle$ is known from $P(d^*(f)/\langle d^*(f)\rangle)$ in each mode and coherence content grows as the function $P(\langle(\phi(f)/\langle\phi(f)\rangle)]$ narrows. The standout feature is that the smaller $\langle\phi(f)\rangle$ or $\langle d^*(f)\rangle$ becomes, the narrower is the spread of the distribution of photon phases $\phi(f)$ present. That is *the phase correlation between photons in an internal mode is increased when the rate of photon annihilation increases*. This is counter-intuitive from a classical perspective where an increase in loss by scattering or friction is associated with less order and a rise in entropy flux. Increased loss by annihilation of quanta in equilibrium is different as it is compensated on average by matching rates of creation. The 2nd Law is not violated as thermal reversibility from reversal of hemispherical output occurs so input and output entropy fluxes match as $(dQ/dt)/T = P_H(T)/T$, with T set by internal recycling. Information and possible partial coherence within thermal emission have been previously noted [9, 11, 23, 24] but relied on Kirchhoff identities and surface sources.

As figure 1 shows photons created beyond a transport distance $d^*(f)_{max} \sim 7.5\langle d^*(f)\rangle \sim 7.5/\alpha(f)$ from an exit interface have negligible chance of exiting. $P(d^*(f))$ and $d^*(f)_{max}$ are qualitatively distinctive if a material is a liquid, conductor, semiconductor, amorphous or crystalline. The schematic of photon creation sets shown in figure 2 is one of many sets of possible photon source emissions in one mode that contribute to internal and external intensity. Outputs are amplified as additional photons emerge into the ground state propagation mode after its temperature has been raised by thermal recycling of internally reflected photons. The rise in intensities as mode photon content is amplified after multiple encounters with hybrid ground state orbitals, adds to heat input.

High internal intensities occur in limited frequency bands within crystalline matter such as SiC and SiO_2, as these modes contain a high linear density of orbitals resulting from hybrids formed with anharmonic lattice distortions. Each local resonance adds local mode density which means extra photons can be accommodated in the hybrid which then re-join the original mode and add to the observed resonant intensity. An example section of a photon standing wave mode containing a regular dense array of hybrid orbitals formed with local anharmonic modes is sketched in the supplement. Lattice oscillations have two distinct components, thermally excited harmonic distortions which propagate as phonons and anharmonic distortions which remain localised

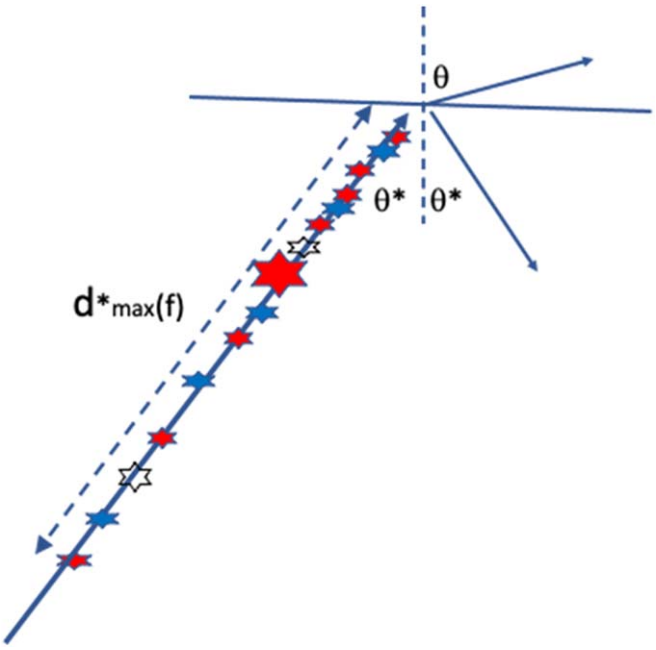

Figure 2. A schematic of one batch of photon creation events within $d^*(f)_{max}$ that exit. Coloured stars represent creation locations within $d^*(f)_{max}$ of an interface. Blue are photons replacing a prior annihilation. The empty star is a 'photon hole' from annihilation not yet replaced and creates a fluctuation in exit intensity. The bright 'star' represents a gain in mode photon flux after passing through a local hybrid mode within $d^*(f)_{max}$.

within their originating bond. These distortions have other roles in thermal physics as they can scatter passing phonons [25]. The resonances seen in thermal radiation from SiO_2 and SiC are between anharmonic energy levels E_A and (E_A+hf). Photons at energy hf then build up locally. This amplification can be also be defined in terms of the phase shift following the local time delay [26, 27] and can be used to experimentally extract the local anharmonic energy for each lattice from external optical data. The supplement has a section containing a basic introduction to virtual-bound-states for this purpose. Previous VBS studies involved s-band free electrons in noble metals hybridising with localised d-orbitals on 3-d atomic impurities.

4. Internal spectral densities and intensities I(f,T)

Each internal ground-state mode has wavevector magnitude $k^* = 2\pi/\lambda^* = 2\pi n(\lambda)/\lambda$ with $n(\lambda)$ the real part of the complex index. $\lambda^* < \lambda$ except inside metals or other materials at wavelengths where $n(\lambda)<1$. If N(f) is the number of photon energy modes whose energy $hf_N < hf$, for N = 1 to N(f), the number of modes at energies between hf and h(f+Δf) is $n^*(hf)\Delta f = dN(f))/df)\Delta f$ with $n^*(hf) = 2n^*_{k*,\sigma}$ the mode density at energy hf from equation (1) for both spins. For large enough samples with no added interior interfaces $n^*(hf)$ is unique to that material. For samples with one or more interior interfaces the principles inside each large material apply except mode contours can change if multiple impacts with an interface are important. Equilibrium balances still apply throughout modes between interfaces, but they must account for photon loss to neighbouring matter at each interface impact, plus gain from mode impacts onto the other side of the same interface. Boundary loss rates from one side at each impact are identical, but different from matter on the opposite side. Thermal radiation displaying resonance features in coated systems where layer thicknesses allow multiple reflections per created photon have been reported [19, 28]. Such structural resonances also occur in our equilibrium approach where mode contours and topology are determined at T = 0 K so the exit direction is into a neighbouring ground-state modes at finite T. The localized hybrid resonances within stoichiometric crystalline matter thus have different origins to structure-based mode resonances between layers. The approach to accurate predictions of intensities exiting transmitting slabs is outlined in the supplement.

For different bulk materials with one interface accurate values of total internal energy U(f,T), uniform internal photon mode currents J(f,T) photons s^{-1} and directional intensities I(f,T,k)=(hf)J(f,T,k) Wm^{-2} for each internal mode, require a correct value of $\rho(hf) = (hf)n^*(hf)$. The expression N(f) based on the spherical symmetry of internal wavevectors $\mathbf{k}^*$ defines the number of empty stationary states within an internal sphere of wavevector radius k^* for each material. $N(f) = (8\pi k^{*3}/3)$ after accounting for opposite spin photons in both half segments of two standing waves. Using optical index n(f)

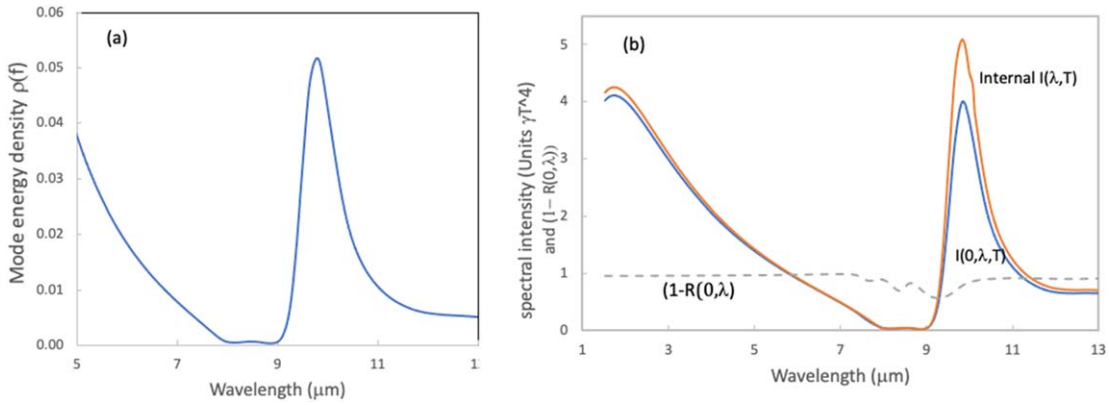

Figure 3. (a) Photon ground state mode density $\rho(hf) = hf^3n(f)^3$ inside silica in units of energy $8\pi h/c^3$ (b) Resulting internal spectral density $\rho(\lambda,T)$ at 300 K (red), and normal emitted intensity $I(0,\lambda,T)$ (blue). Intensity units are $8\pi k^4/(c^3h^3)]T^4$ and are universal. The blue plot in (b) is a close fit to observed normal intensities. Emissivity $\varepsilon(0^*,f) = (1\text{-}R(0,f))$ the dashed plot and is the only case where external reflectance can be used. Silica optical constants are from Kischkat *et al* [35].

$$N(f) = \frac{8\pi f^3 n(f)^3}{3c^3} = N_{BB}(f)n(f)^3 \tag{6}$$

The cavity standing wave density $N_{BB}(f) = (8\pi f^3/3c^3)$ applies by itself only when index $n(f) = 1$. Calculating $(hf)[dN(f)/df]$ yields two separate terms. The second adds the term $3N_{BB}(f)n(f)^2hf(dn(f)/df)$ which we drop at this point as its contribution to photon density at finite T, as shown in the supplement, is negligibly small relative to that from the remaining energy density term in equation (6). The energy level density $\rho(hf) = 2(hf)n_{k^*,\sigma}$ from equation (1) with all internal fluxes in thermal equilibrium unpolarised is

$$\rho(hf) = 2(hf)n_{k*,\sigma} = \frac{8\pi hf^3 n(f)^3}{c^3} = \rho_{BB}(hf)n(f)^3 \tag{7}$$

and $\rho_{BB}(hf)=(hf)[dN_{BB}(f)/df]$. The internal intensity I(f,T) for bulk samples equals the contribution per mode to photon volume density $N(f,T) = \rho(hf)f_{BE}(f,T)$ with $f_{BE}(f,T) = [\exp(hf/kT)-1]^{-1}$ the Bose–Einstein occupancy factor. Converting the internal photon densities N(f,T) and intensity I(f,T) to functions of dimensionless energy units $x(f,T) = hf/kT$, yields both internal spectral intensity I(f,T) and the contribution of each modes spectral energy density to internal energy U(T)

$$I(f,\ T) = I(x) = \frac{x^3n(x)^3}{(\exp(x)\ -\ 1)}\gamma T^4\ Wm^{-2} \tag{8}$$

$\gamma = 8\pi k^4/c^3h^3 = \sigma(15/\pi^4)$ with *0.15399σ replacing the Stefan-Boltzmann constant for internally generated photons*. The expression for $I_{BB}(x)$ inside a cavity occurs only when $n(x) = 1$ and as Planck found $I_{BB}(x) = \{x^3/[\exp(x)-1]\}\gamma T^4$. The photonic contribution to internal energy U(f,T) within solid or liquid matter thus requires integrating of equation (8) over all x. When $n(x) = 1$ the integration yields $U(f,T) = 6.4939\gamma T^4 = \sigma T^4$. Within matter integration of equation (8) yields the material specific multiple $\kappa\gamma T^4$ where κ can be of order 6.5 when n(x) is near 1.0, but is often significantly different. The non-reciprocal emissivity we derive in section 5 adds an additional shift in spectral response. An example of the empty mode energy density $n_{k^*,\sigma}$ based on equation (7) is in figure 1(a) for silica and the resulting photon spectral density N(f,T) calculated using equation (8) at 300 K is in figure 1(b). Figure (2) for water contains plots of $I(f,T) = (hf)N(f,T)$ at 300 K and 360 K, plus normally emitted intensity I(0,f,T) at 300 K as then $1\text{-}R(0^*,f) = 1\text{-}R(0,f)$. Internal propagation preceding emission thus adds important modifications to the Planck-Kirchhoff results in current use. Internally generated spectral intensities operated on by thermal emissivity are unique to each material. The second modification required is that oblique exit intensities have been refracted. For two element compounds with known complex indices in the IR, fluxes modelled provide convincing experimental validation that emissivity is internally defined and non-reciprocal.

The IR optical data available and used for silica and water in figures 3 and 4 unfortunately did not cover all wavelengths needed to completely define internal $I_H(T)$ with equation (8). Over the range we had index data integration meant $\kappa_{water} > 8.52$. To relate to past calorimetric data and radiant loss calculations that assumed $P_H(T) = \varepsilon_{H,K}\sigma T^4$ we equate the correct result $P_H(T) = \varepsilon_H\kappa\gamma T^4$ and replace γ with $\sigma/6.4939$. For water approximate extrapolation of the plot in figure 4 at 300 K indicates that κ lies between 9 and 10 and that $\kappa\gamma>\sigma$. Based on past calorimetric estimates of $\varepsilon_{H,K}\sigma$ from rate of heat loss by radiation from smooth water and writing $\varepsilon_H = P_H(T)/\kappa\gamma T^4$ we estimate $0.92>\varepsilon_H > 0.85$. This range of ε_H is compatible with the expected high radiant cooling rates $P_H(T)$ from smooth water. Our predicted external spectral intensities from equation (8) do

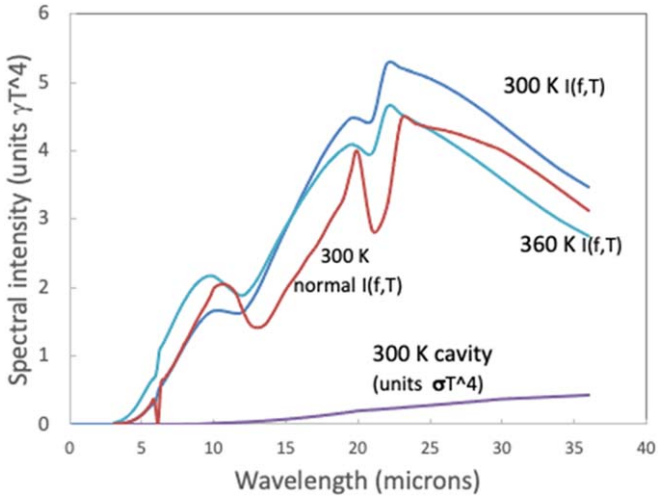

Figure 4. Spectral intensity at 300 K and 360 K within still water (blue) with the resulting normal exit intensity at 300 K (red). Internal intensities in water display local photon resonances with water's four dominant molecular oscillation modes [32]. Cavity intensities lack strong resonant features can be compared using the factor $6.4939/\kappa$ introduced in section 2 for each internal intensity I(f,T). For water equation (8) with interface projection factor $\cos\theta^*$ the value of κ is above 8.52. n(f), k(f) data used is from Hale *et al* [36].

duplicate the variety of complex IR spectral intensities observed exiting water [29, 30] and other compound materials as seen in remote sensing where overlapping internal resonances are commonplace. Modes that form hybrids with photon modes in liquids are localised on molecules. Resonance linked to molecular mode oscillations in water are seen in figure (3) using equation (8) with correct emissivity. Our spectral predictions are in excellent agreement with reported data from remote sensing studies [12, 29–31]. For water reliable radiant loss models are of major environmental importance and display VBS resonances at water's four main molecular vibration modes [32]. These and the hybrid resonances in crystalline materials with anharmonic distortions means IR thermal intensity data and thermal image spectra can map materials within a mix. Both allow intensity data to be used for precision chemical analysis and the identification of molecular modes. Water's four resonant bands within thermal emission exemplify a common feature in thermal radiation from dielectric solids and liquids. They occur at energies that allow photon propagation modes and local oscillator or defect modes to add a local hybrid oscillator to ground state modes. Propagating photons 'enter' each hybrid orbital for a brief period. Over the short delay the extra photons produced finally enter the original basic mode, with a jump in phase and final energy flux. Photon and local oscillator momentum are conserved. Events like this in condensed matter physics are labelled 'virtual-bound-states' (VBS) [26, 33, 34].

While photon internal density of states from equations (6), (8) depends on $n(f)^3$ and T, internal mode reflectance, external transmittance and emissivity depend on n(f), and k(f) the mode's attenuating index. Refraction of the transmitted part of projected intensity $\mathbf{I}(f,T)\cos\theta^*$ after projection of each I(f,T) onto an exit interface in direction θ^* to the normal, defines emissivity. As illustrated schematically in the supplement the reversal of the flux emerging in direction θ to the normal cannot reproduce the reversal of originating internal intensity $\mathbf{I}(\theta^*,f,T)$ as required by the Kirchhoff rule. Internal ground state fluxes are reversible if their $k(f) = 0$, but once occupied most mode exit intensities are irreversible. Optical irreversibility of each different exit intensity $I(\theta,f,T)$, as noted above, does not prevent thermodynamic reversal to the original equilibrium state if the *entire hemispherical radiant power $P_H(T)$ is reversed and the original dQ/dt source is removed* (initially or over time).

Another important difference to emission from a cavity compared to that from matter after refraction is that the range of frequency modes exiting depends for matter on the frequency dependence of internal critical angles $\theta^*_C(f)$. For some materials including plasmonic metals total internal reflection (TIR) is absent [37–39], but for many dielectrics $\theta^*_C(f)$ plays a key role in emission. This is demonstrated in section 5, where our emissivity models are applied to refraction of radiation exiting bulk silica. Exit intensity directional profiles modelled for a few fixed θ^* values vary widely as a function of mode frequency and a reciprocal emissivity cannot predict such behaviour. For dielectrics and for very hot matter refraction and TIR both influence emissivity. In some frequency bands exit intensity directions are anomalous as their exit direction $\theta < \theta^*$ for a limited f range after emissivity acts on internal projected intensity $I(\theta^*,f,T)\cos\theta^*$.

When internal mode photons are subject to annihilation, exit refracted intensities cannot be reversed. The resulting non-reciprocal emissivity is formally derived from first principles using equations (1)) in the next section. Spherical symmetry of all internal ground state modes means internal intensities I(f,T) are uniform in all

internal directions. Ground state standing waves contain **J**(f,T,+**k**) and opposite flow **J**(f,T,-**k**), with half of each for up spin photons and half for down spin. This means Planck's addition of an extra factor 2.0 for exit fluxes was not justified, and would not have been needed had he not modulated cavity emission intensities with the factor '$\cos\theta$' as observed by Lambert [3] in his study of thermal emission from a heated metal ribbon. The emissivity replacement rules derived in the next section indicate that a '$\cos\theta$' factor always multiplies intensities exiting a smooth interface and is due to the refraction required for *conservation of exiting photon momentum*. The one exception is intensity exiting a hole in a cavity wall as its internal fluxes exit without change of direction. For a contoured or rough surface, angle θ^* is relative to the surface normal at each small area where an oblique incident photon tunnels through the interface reaction potential. In that case the '$\cos\theta$' rule applies locally. Planck's 2.0 is absent from all emission models when internal propagation precedes photon emission.

5. Models for the non-reciprocal emissivity

While photon internal mode density from equation (6) depends only on the real part of each material's complex index n(f), internal reflectance, external transmittance and emissivity depend on both n(f) and k(f) with k(f) a function of T hence of photon density in its mode. Exit intensity $\mathbf{I}(\theta,f,T)$ flows within the external ground state mode in free space in direction θ to the local normal that ensures momentum conservation. It is the transmitted part of internal projected intensity $I(\theta^*,f,T) = I(f,T)\cos\theta^*$. Whenever index k(f) within an occupied internal mode is finite, its value determines the direction of the neighbouring mode its emitted photons enter. The resulting expression for emissivity derived here is then non-reciprocal. Optical irreversibility of $I(\theta,f,T)$ does not however prevent optical and thermal reversibility of emitted hemispherical power $P_H(T)$ provided original heating rate dQ/dt is removed. Another difference to emission from a cavity is that the range of frequency modes exiting depends also for matter on interface structure and the frequency dependence of critical internal angles $\theta^*_C(f)$. For some materials, including plasmonic metals, total internal reflection is absent, but for many dielectrics it spans specific frequency bands at fixed internal directions θ^*. We will demonstrate this by modelling select $\theta(f)$ after refraction of internally occupied modes exiting silica in section (6). A complex mix of exit directions results as frequency changes when θ^* is fixed. The Kirchhoff emissivity plus surface sources cannot predict such outcomes. In dielectrics and in very hot matter refraction not only involves TIR, but in some bands exit intensity directions are anomalous as $\theta(f)<\theta^*(f)$. This occurs as select exit intensities move closer to the normal than the internal angle of incidence which occurs either when $n(f) < k(f)$ (as in plasmonic conductors and dielectric Restrahlen bands), or when $n(f) > k(f)$ but they are close. Since k(f) usually rises as temperature increases the prevalence of anomalous refraction is expected to increase with ongoing rise in T. An important example is exit intensities from stable plasmas as we expect them to cluster close to the normal to each plasma's boundaries. Our models in section 2 imply that at very high T a high degree of directional coherence in output fluxes is possible without invoking Zernicke [40] classical interference for a stable plasma in equilibrium. A rough plasma boundary is a non-equilibrium feature and produces random emissions in time and space. After travelling some distance into the continuum its spatial randomness will follow Zernicke's predictions and finally reproduce the expected spatial coherence.

If an externally applied thermal gradient dT(x)/dx is present the steady state diffusion of heat and of photons can be based on a series of elemental equilibrium states where photon densities are N(f,T(x)) at $T(x) = [dT(x)/dx]\Delta x$. A photon density gradient dN(f,T(x))/dx adds a photon diffusion current which does not transport heat, but local thermal equilibrium means that $(dN(f,T(x))/dx)\Delta x = [dM(f,T(x))/dx]\Delta x$. The gradient [dM(f,T(x))/dx] is additional to that driving heat flux from diffusion of phonons in the absence of photons. Detailed balance within each Δx segment sets local equilibrium. As a result photon density gradients dN(f,T(x))/dx per mode 'drag' phonons which add to the heat flow. Phonon drag of electron fluxes was postulated by Peierls [41] but his predictions of a T^5 dependence for low T electron currents was not observed. A contribution to heat flow from photon drag of phonons is expected in select materials as a function of temperature T(x).

All exit intensities reduce to the form $I(\theta,f,T) = \varepsilon(\theta,f)I(f,T)\cos\theta$ which depends on the relation between θ and θ^* due to refraction. The small interface areas each hemispherical set of ground state photons converge to are of order a collision cross-section with the interface reaction potential, or about a bond length ($\sim 10^{-10}$ m) across. Emissivity acts on each projection $I(f,T)\cos\theta^*$. Two different identities for $I(\theta,f,T)$ arise and must produce the same exit intensity. First $I(\theta,f,T) = [1-R(\theta^*,f)]I(f,T)\cos\theta^*$ with $R(\theta^*,f)$ internal spectral reflectance, second $I(\theta,f,T)=T(\theta^*,\theta,f)I(f,T)\cos\theta^*$ with $T(\theta^*,\theta,f)$ the flux transmittance. Conservation of energy and momentum is then ensured by the identities in equations (9), (10). The expression $I(\theta,f,T) = \varepsilon(\theta,f)I(f,T)\cos\theta$ for external intensity comes from the final expression in equation (9) operating on $I(f,T)\cos\theta^*$ so that $|t(\theta^*,f)|^2 = \varepsilon(\theta,f)$. Replacing $(1-R(\theta^*,f))$ with $\varepsilon(\theta^*,f)$ results in the alternate definition of emissivities in equation (11). The contribution of refraction to emissivity comes from the ratio $\cos\theta/\cos\theta^*$. A condensed conservation relation after refraction is $\varepsilon(\theta^*,f)\cos\theta^* = \varepsilon(\theta,f)\cos\theta$.

$$(1 - R(\theta^*, f)) = T(\theta^*, \theta, f) = |t(\theta^*, \theta, f)|^2(\cos\theta/\cos\theta^*) \quad (9)$$

$$I(\theta, f, T) = \varepsilon(\theta^*, f)I(f, T)\cos\theta^* = \varepsilon(\theta, f)I(f, T)\cos\theta \quad (10)$$

Since $\varepsilon(\theta,f) = |t(\theta^*,f)|^2$ defines emissivity with internal incidence angle used in a standard Fresnel amplitude coefficient it is straightforward to show that oblique $\varepsilon(\theta,f)$ never matches $A(\theta,f)$. Inclusion of the polarisation of internally reflected photons is required by equilibrium thermal balances and the two non-reciprocal emissivity expressions

$$\varepsilon_{TM}(\theta, f) = |t_{TM}(\theta^*, f)|^2;\ \varepsilon_{TE}(\theta, f) = |t_{TE}(\theta^*, f)|^2 \quad (11)$$

Expressions for the Fresnel transmission and reflection coefficients for absorbing media are treated in many optical texts [42–44] and embedded in thin film software packages. θ^* and complex indices n(f) and k(f), model each $R(\theta^*,f)$ and $\varepsilon(\theta^*,f)$. Observations of two or more exit intensities based on equation (8) for internal I(f,T) allows a material's complex indices at each wavelength to be extracted from a small number of observed intensities exiting in different directions. This is one validation test for this paper's models if the emitting sample's indices are known. Figures 3 and 4 were examples of successful theoretical and experimental validation tests.

To sum all external radiance elements to establish $P_H(T)$ the role of solid angle changes due to refraction must be included in radiance conservation rules. That is done in section 7. Steradian changes are essential to correct modelling of external radiance.

6. The impacts of TIR and anomalous refraction on exit intensities

To model spectral and directional outcomes defined by $I(\theta,f,T)$ expressions linking internal $\theta^*(f)$ to externally observed $\theta(f)$ are needed to establish $|t(\theta^*,f)|^2$. There are two ways this can be done. A recently established approach is to use a complex Snell's Law [38, 39] recently derived for EM waves crossing the exit interface from within an absorber into another material or into the continuum. Expressions resulting from applying the usual interface boundary conditions are more complex than those in Born and Wolff [42] for external waves incident onto an absorber. The conservation rules from equations (9)) can also be used in place of complex Snell's Laws. If n(f) and k(f) are known all Fresnel coefficients needed can be evaluated then used to link $\theta^*(f)$ and $\theta(f)$ since

$$\cos\theta(f) = \frac{(1 - |r_{TE}(\theta^*, f)|^2)\cos\theta^*(f)}{|t_{TE}(\theta^*, f)|^2} = \frac{(1 - |r_{TM}(\theta^*, f)|^2)\cos\theta^*(f)}{|t_{TM}(\theta^*, f)|^2} \quad (12)$$

If exit direction and exit intensity are known from experimental observations of $I(\theta,f,T)$ a solution or fit to θ^* becomes possible.

It is instructive to study how $\theta(f)$ and $I(\theta,f,T)$ vary as a function of mode frequency for fixed θ^*. Spectral exit intensities from each fixed θ^* direction experience an interesting, and important array of directional outcomes from absorbing materials as frequency changes. Examples are plotted in figure 5 for silica of $\theta(f)$ from three fixed internal incident directions θ^*. The frequencies chosen are for internal mode intensities at 300 K. Distinct frequency bands display the following sets of behaviour at fixed θ^*; regular refraction, total internal reflection (TIR), and anomalous clustering of exit intensities close to the normal. The latter are labelled 'anomalous refraction' since the exit direction is closer to the normal than incident direction θ^*. Within dielectrics infra-red critical angles are often around 45° as seen in figure 5 for silica. Anomalous clustering near normal exit directions is also expected for plasmonic metals from recent studies of intensities exiting silver [37, 38]. For metals and for dielectrics these refraction anomalies occur in spectral zones where $k(f) > n(f)$, or when $n(f) > k(f)$ but they are close. A large increase in k(f) is expected within hot plasmas, so that equilibrium exit fluxes also cluster near the normal for an intense narrowly spaced set of intensities close to the normal to a stable plasma's edges. If the plasma is a sphere in equilibrium near normal directional coherence can explain for example the very small half-angle spread of solar intensities impacting our atmosphere despite the distance travelled to earth.

7. Exit radiance and conclusion

Exiting optical fluxes diverge so cooling rates requires consideration of the exit radiance after refraction resulting from internal radiance elements $\Delta\Lambda(f,T)\ Wm^{-2}Sr^{-1}$. Like I(f,T) internal radiance elements $\Delta\Lambda(f,T)$ are spherically symmetric in bulk matter at each frequency. Photons within modes making up $\Delta\Lambda(f,T)$ obey the same statistics and transport rules as single modes so internal solid angles $\Delta\Omega^*$ Sr are uniform and exit radiance has elements $\Delta\Lambda(\theta,\phi\ f,T)=[\Delta I(\theta,f,T)/\Delta\Omega(\theta,\phi)]\ Wm^{-2}Sr^{-1}$ after emissivity acts on the projection internally of $\Delta\Lambda(f,T)$ onto the interface for projected radiance $\Delta\Lambda(\theta^*,f,T) = \Delta\Lambda(f,T)\cos\theta^*$. The fixed internal solid angle $\Delta\Omega^*$ Sr means the internal spherical radiance element crossing through a small sphere is $(4\pi/\Delta\Omega^*)\Delta\Lambda(f,T)$ so $(2\pi/\Delta\Omega^*)\Delta\Lambda(f,T)\ Wm^{-2}Sr^{-1}$ impacts the interface over many small areas. The energy-momentum

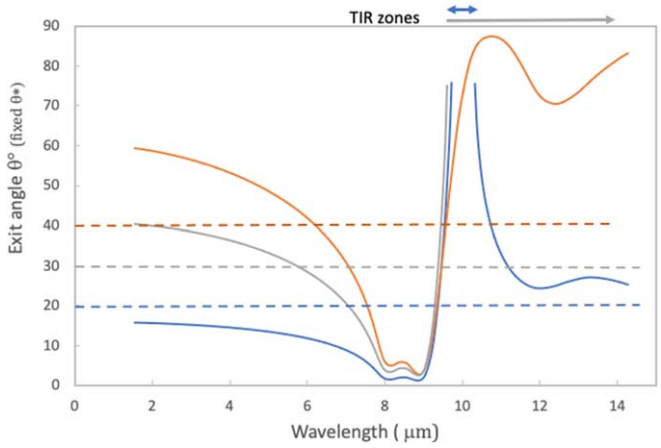

Figure 5. The spectral dependence of exit directions for three fixed internal impact directions θ^* (at the dashed lines) at 20°, 30° and 40° onto a smooth silica interface. The TIR band when $\theta^* = 20°$ (blue) is confined to the range 9 μm to 11 μm. In contrast for $\theta^* = 30°$ (grey) the TIR zone starts at $\sim$ 9 μm but is not truncated by 15 μm. For $\theta^* > 46°$ in silica internal photons with $\lambda > 1$ μm experience TIR.

conservation rule for emitted radiance then accounts for three geometric changes. They are internal to exit direction θ^* to θ, internal to exit cross-sections dA* to dA(θ,ϕ), and internal solid angles $\Delta\Omega^*$ to $\Delta\Omega(\theta,\phi)$. The dependence of $\Delta\Lambda(\theta,\phi$,f,T) on $\Delta\Lambda(\theta^*$,f,T) derived as above for intensity to conserve energy and momentum is in equation (13). A dependence on θ^* and ϕ^* is initially included this time to allow for possible anisotropy in emissivity and internal reflectance when R(θ^*,ϕ^*,f) is dependent on ϕ^*. With internal annihilation rates of photons required to balance internal reflection rates the radiance conservation rule now becomes

$$\frac{d\Lambda(\theta,\ \phi,\ \mathrm{f},\ \mathrm{T})}{d\Lambda(\mathrm{f},\ \mathrm{T})} = \varepsilon(\theta^*,\ \phi^*,\ \mathrm{f})\cos\theta^*\sin\theta^* d\theta^* d\phi^* = \varepsilon(\theta,\ \phi,\ \mathrm{f})\cos\theta sin\theta d\theta d\phi \tag{13}$$

For smooth surfaces dϕ^* and dϕ in equation (13) cancel and the radiance conservation rule reduces to $\varepsilon(\theta^*$,f)cos θ^*d$\Omega(\theta^*) = \varepsilon(\theta$,f)cos$\theta$d$\Omega(\theta)$ for each polarisation with d$\Omega(\theta) = \sin\theta$d$\theta$, and d$\Omega(\theta^*)$ set at a constant internal but small steradian value.

The ratio [$\Delta\Omega(\theta$,f)/$\Delta\Omega^*$(f)] varies as exit direction θ changes due to refraction. It can be evaluated once the value of θ(f) has been determined for each internal radiance impact direction θ^* as above. The extent of change in this ratio can be quite large and plays an important role in the exit radiance components making up hemispherical emittance ε_H, which total to cooling rate P_H(T). Across anomalous refraction zones the ratio [$\Delta\Omega(\theta$,f)/$\Delta\Omega^*$] contracts near to the normal so that near normal intensity can be intense. With axial symmetry equation (10) for P_H(T) results with $\varepsilon(\theta$,f) defined as before and dΛ(f,T) material specific replacing dΛ_{BB}(f,T) means

$$P_H(T) = 2\pi\Lambda_H(T) = \int_0^{2\pi} d\Omega(\theta)\int_0^{\infty} df\varepsilon(\theta,\ f)d\Lambda(\mathrm{f},\ \mathrm{T})\cos\theta = \varepsilon_H\kappa\gamma T^4 \tag{14}$$

This expression or equation (8) provides correction factors to past predictions based on the Kirchhoff-Planck approach. Errors can be small as indicated above for water but are always finite and sometimes significant. Lambert's data was correct but his use of surface sources to explain it instead of refraction was incorrect, and was unfortunately adopted by Planck and many others. A large amount of carefully acquired calorimetric emittance data since the 1950's to today could not be reproduced with optical calculations based on the Kirchhoff-Planck optical models. This paper's models rectify that problem. A selection of such studies [45–49] are referenced. Many errors were attributed to unidentified experimental errors despite the careful analysis of possible error contributions that had been carried out. Their problem was instead the use of Kirchhoff-Planck intensity relations.

References and a Glossary summarising all main concepts

Symbol/Term	Definition
n(f)	ground state standing wave phase index, real part of EM wave index
k(f)	photon dissipation index per mode, imaginary part of EM wave index
$\varepsilon(\theta$,f)	spectral emissivity for fluxes in exit direction θ to local normal
$\varepsilon(\theta^*$,f)	[1-R(θ^*,f)] at internal impact direction θ^* to local normal
$n_{k^*,\sigma}$	mode density at internal wavevector k* for spin σ photons
k*(f)	2πn(λ)/λ, the internal wavevector of each ground state mode

(Continued.)

Symbol/Term	Definition
R_H	internal hemispherical reflectance
T	sample equilibrium temperature
γ	universal constant, $8\pi k^4/c^3h^3 = (15/\pi^4)\sigma = 0.15399\sigma$
σ	Stefan-Boltzmann constant (cavity emission only)
N(f,T)	internal density of photons per mode at T
M(f,T)	internal density of excitations that create and annihilate photons
dQ/dt	sample external heating rate
dQ^*/dt	total internal heating rate due to photon thermal recycling
I(f,T)	internal intensity at f and T in all directions
$I(\theta^*,f,T)$	$I(f,T)\cos\theta^*$, Internal intensity projected onto the interface
$\Delta\Lambda(f,T)$	internal spectral radiance element at f and T in all directions
$\Delta\Lambda(\theta^*,f,T)$	$\Delta\Lambda(f,T)\cos\theta^*$ $Wm^{-2}Sr^{-1}$ radiance projection onto an interface
$\Delta\Lambda(\theta,\phi,f,T)$	external directional radiance at f and T
$d^*(f)$	internal distance travelled by each photon since its creation
$\langle d^*(f)\rangle$	mean-free-path per mode (inverse of absorption coefficient $\alpha(f)^{-1}$)
$d^*(f)_{max}$	beyond $d^*(f)_{max}$ photon survival probability is negligibly small
$P[d^*(f)]$	photon survival probability with distance travelled from creation
y(f)	$d^*(f)/\langle d^*(f)\rangle$
x(f,T)	hf/kT
$\rho(d^*(f))$	density of photons at $d^*(f)$ between $d^*(f)$ to $[d^*(f)+\Delta d^*(f)]$ per mode
$A(\theta,f)$	absorptance of reversed exit flux, also the Kirchhoff emissivity
ε_H	reversible hemispherical emittance (based on irreversible $I(\theta,f,T)$)
$\Delta\phi(f)$, $\langle\Delta\phi(f)\rangle$	phase change and mean-phase-change per photon since creation
C(T)	sample thermal mass without photon recycling by an interface
$C^*(T)$	hybrid thermal mass based on dQ/dt with photon thermal recycling
$t_{TM}(\theta^*,f)$, $t_{TE}(\theta^*,f)$	Fresnel complex transmittance coefficients for polarised emission
$\Delta\Omega^*$, $\Delta\Omega(\theta,\phi)$	common internal radiance solid angle element, refracted steradians
dA^*, $dA(\theta,\phi)$	common internal, exit directed external cross-sections per intensity
N(f)	$8\pi f^3 n(f)^3/3c^3$, the number of modes whose energy is below hf
$f_{BE}(f,T)$	$1/[\exp(hf/kT)-1]$, the Bose–Einstein occupation factor per mode
U(T)	internal energy density from all excited quanta including photons
$\mathbf{J}(f,T,\mathbf{k}^*)$, $\mathbf{J}(f,T,\mathbf{k})$	internal and external photon flux vector 'current densities'
dT(x)/dx	externally imposed thermal gradient in x-direction
TIR	total internal reflectance
VBS	virtual-bound-state between a photon mode and a local oscillator
E_A	anharmonic oscillator energies that hybridise with photon modes
FDT	fluctuation-dissipation-theory (the semi-classical approach to the consequences of annihilation and creation of excited quanta)

Data availability statement

All data that support the findings of this study are included within the article (and any supplementary files).

ORCID iDs

G B Smith https://orcid.org/0000-0002-6985-2880
A R Gentle https://orcid.org/0000-0001-8964-0722
M D Arnold https://orcid.org/0000-0003-4164-0242

References

[1] Planck Max 1998 *Eight bLectures on theoretical physics* (New York: Dover Publications) Eight lectures on theoretical physics: courier corporation
[2] Planck M 1914 *The Theory of Heat Radiation, English translation by M Morton* (Philadelphia: P. Blakiston's Son & Co)
[3] Lambert J H 1760 *Photometria, sive de Mensura et Gradibus Luminis* (Augsburg: Colorum et Umbrae)
[4] Kirchhoff G I 1860 On the relation between the radiating and absorbing powers of different bodies for light and heat *The London, Edinburgh, and Dublin Philosophical Magazine and Journal of Science.* **20** 1–21
[5] Shen L-T, Yang Z-B, Wu H-Z, Chen X-Y and Zheng S-B 2012 Control of two-atom entanglement with two thermal fields in coupled cavities *JOSA B.* **29** 2379–85

[6] Shen L-T, Yang Z-B, Wu H-Z and Zheng S-B 2017 Quantum phase transition and quench dynamics in the anisotropic Rabi model *Phys. Rev. A* **95** 013819
[7] Shen L-T, Yang J-W, Zhong Z-R, Yang Z-B and Zheng S-B 2021 Quantum phase transition and quench dynamics in the two-mode Rabi model *Phys. Rev. A* **104** 063703
[8] Rytov S M 1959 Theory of electric fluctuations and thermal radiation Air force Cambridge Research Labs Hanscom AFB MA;
[9] Kish L B and Granqvist C G 2014 On the security of the Kirchhoff-law–Johnson-noise (KLJN) communicator *Quantum Inf. Process.* **13** 2213–9
[10] Polimeridis A G, Reid M H, Jin W, Johnson S G, White J K and Rodriguez A W 2015 Fluctuating volume-current formulation of electromagnetic fluctuations in inhomogeneous media: incandescence and luminescence in arbitrary geometries *Physical Review B.* **92** 134202
[11] Greffet J-J, Carminati R, Joulain K, Mulet J-P, Mainguy S and Chen Y 2002 Coherent emission of light by thermal sources *Nature* **416** 61
[12] Wenrich M L and Christensen P R 1996 Optical constants of minerals derived from emission spectroscopy: application to quartz *Journal of Geophysical Research: Solid Earth.* **101** 15921–31
[13] Bilokur M, Gentle A, Arnold M, Cortie M and Smith G 2019 High temperature optically stable spectrally-selective Ti1-xAlxN-based multilayer coating for concentrated solar thermal applications *Sol. Energy Mater. Sol. Cells* **200** 109964
[14] Smith G, Swift P and Bendavid A 1999 TiN x films with metallic behavior at high N/Ti ratios for better solar control windows *Appl. Phys. Lett.* **75** 630–2
[15] Bilokur M 2019 Optical thin film stacks integrating spectral and angular control of solar energy and thermal radiation *Phd Thesis* University of Technology Sydney https://opus.lib.uts.edu.au/handle/10453/137062
[16] Cagran C P, Hanssen L M, Noorma M, Gura A V and Mekhontsev S N 2007 Temperature-resolved infrared spectral emissivity of SiC and Pt–10Rh for temperatures up to 900 °C *Int. J. Thermophys.* **28** 581–97
[17] Lawrence E O 1926 Transition probabilities: their relation to thermionic emission and the photo-electric effect *Phys. Rev.* **27** 555
[18] McMahon H 1950 Thermal radiation from partially transparent reflecting bodies *JOSA.* **40** 376–80
[19] Kollyukh O, Liptuga A, Morozhenko V and Pipa V 2003 Thermal radiation of plane-parallel semitransparent layers *Opt. Commun.* **225** 349–52
[20] Mishchenko M I editor 125 years of radiative transfer: enduring triumphs and persisting misconceptions *AIP Conf. Proc.; 2013: American Institute of Physics.*
[21] Mishchenko M I 2014 Directional radiometry and radiative transfer: the convoluted path from centuries-old phenomenology to physical optics *J. Quant. Spectrosc. Radiat. Transfer* **146** 4–33
[22] Sears F and Salinger G 1976 *Thermodynamics, Kinetic Theory and Statistical Thermodynamics* 3rd (Reading, Mass. USA: Addison Wesley Pub. Co)
[23] Kish LB and Granqvist C-G. Electrical Maxwell demon and Szilard engine utilizing Johnson noise, measurement, logic and control 2012
[24] Greffet J-J, Bouchon P, Brucoli G, Sakat E and Marquier F 2018 Light Emission by Nonequilibrium Bodies: Local Kirchhoff Law. *Phys Rev X* **8** 021008
[25] Ashcroft N W and Mermin N D 1976 *Solid State Physics: Holt* (new york London: rinehart and winston)
[26] Friedel J 1956 On some electrical and magnetic properties of metallic solid solutions *Can. J. Phys.* **34** 1190–211
[27] Rivier N and Zuckermann M 1968 Equivalence of localized spin fluctuations and the Kondo-Nagaoka spin-compensated state *Phys. Rev. Lett.* **21** 904
[28] Ben-Abdallah P 2004 Thermal antenna behavior for thin-film structures *J. Opt. Soc. Am. A* **21** 1368–71
[29] Michalski J R, Cuadros J, Niles P B, Parnell J, Rogers A D and Wright S P 2013 Groundwater activity on mars and implications for a deep biosphere *Nat. Geosci.* **6** 133–8
[30] Smith W L *et al* 1996 Observations of the infrared radiative properties of the ocean–implications for the measurement of sea surface temperature via satellite remote sensing *Bull. Am. Meteorol. Soc.* **77** 41–52
[31] Vaughan R G, Calvin W M and Taranik J V 2003 SEBASS hyperspectral thermal infrared data: surface emissivity measurement and mineral mapping *Remote Sens. Environ.* **85** 48–63
[32] Brubach J-B, Mermet A, Filabozzi A, Gerschel A and Roy P 2005 Signatures of the hydrogen bonding in the infrared bands of water *J. Chem. Phys.* **122** 184509
[33] Hubbard J 1964 Electron correlations in narrow energy bands. II. The degenerate band case *Proceedings of the Royal Society of London Series A Mathematical and Physical Sciences.* **277** 237–59
[34] Anderson P W 1978 Local moments and localized states *Rev. Mod. Phys.* **50** 191
[35] Kischkat J *et al* 2012 Mid-infrared optical properties of thin films of aluminum oxide, titanium dioxide, silicon dioxide, aluminum nitride, and silicon nitride *Appl. Opt.* **51** 6789–98
[36] Hale G M and Querry M 1973 Optical constants of water in the 200-nm to 200-μm wavelength region *Appl. Opt.* **12** 555–63
[37] Zhang S, Liu L and Liu Y 2020 Generalized laws of Snell, Fresnel and energy balance for a charged planar interface between lossy media *J. Quant. Spectrosc. Radiat. Transfer* **245** 106903
[38] Zhang Q 2015 The refractive angle of light propagation at absorbing media interface *Optik* **126** 4387–91
[39] Shen J, Yu H and Lu J 2010 Light propagation and reflection-refraction event in absorbing media *Chin Opt Lett.* **8** 111–4
[40] Zernike F 1938 The concept of degree of coherence and its application to optical problems *Physica* **5** 785–95
[41] Peierls R 1932 Zur theorie der absorptionsspektren fester Körper *Ann. Phys. (Berlin)* **405** 905–52
[42] Born M and Wolf E 2013 *Principles of Optics: Electromagnetic Theory of Propagation, Interference and Diffraction of Light* (Amsterdam: Elsevier)
[43] Macleod H A 2010 *Thin-Film Optical Filters* 4th (Boca Raton: CRC press) (https://doi.org/10.1201/9781420073034)
[44] Strong J 1955 *Optical Properties of Thin Solid Films. OS Heavens.* (New York; Butterworths, London: : Academic) vii+261 pp. Illus. $6. Science. 1955;122(3177):974-5.
[45] Abbott G 1962 Total normal and total hemispherical emittance of polished metals. DTIC Document WADD-TR-61-94 Part II Report No.: DTIC Document # WADD-TR-61-94 Part II Contract No.: WADD-TR-61-94 Part II.
[46] Curtis H B 1966 Measurement of emittance and absorptance of selected materials between 280 deg and 600 deg K *J. Spacecr. Rockets* **3** 383–7
[47] Hamilton D C and Morgan W 1952 Radiant-interchange configuration factors NASA technical note 2836
[48] Willrath H and Smith G 1980 A new transient temperature emissometer *Sol. Energy Mater.* **4** 31–46
[49] Králík T, Musilová V, Hanzelka P and Frolec J 2016 Method for measurement of emissivity and absorptivity of highly reflective surfaces from 20 K to room temperatures *Metrologia* **53** 743